Technical Report 1611
June 1993

Marine-Modified LOWTRAN: The Contribution of Sun Glint

C. R. Zeisse

Approved for Public Release; Distribution is Unlimited

SUMMARY

OBJECTIVE

LOWTRAN, a computer code that predicts infrared properties of the atmosphere, is primarily intended for aerial and terrestrial applications. LOWTRAN has recently been modified to improve its predictive ability in marine environments. The objective of this report was to describe a further improvement in the marine modifications. Sun glint, the specular reflection of solar rays by the ocean surface into the observer's line of sight, has been included. The glint model is based on the ocean wave slope statistics of Cox and Munk (1954).

RESULTS

The results of the modified model have been compared with infrared data taken at 3 to 5 microns over the open ocean under various conditions of solar elevation and wind speed. A significant glint contribution was obtained under the prevailing conditions for one data set: 1450 PDT on 10 October 1991. A close match existed between the *shape* of the predicted and observed radiance values in the ocean sky and sea, but the *absolute value* of the predicted and observed radiances differed by a large constant whose equivalent blackbody temperature was on the order of 5°C. The origin of this additional radiance is unknown. It may be multiple scattering of solar radiation.

CONTENTS

INTRODUCTION 1

MARINE MODIFICATION OF LOWTRAN 6 1

SUN GLINT 2

SUN GLINT FORMULATION 11

DETAILS OF THE FORMULATION 15

FORTRAN CODING 21

COMPARISON WITH EXPERIMENT 23

CONCLUSION 28

REFERENCES 29

APPENDIX A DERIVATION OF GEOMETRIC EQUATIONS GOVERNING THE REFLECTION OF RADIATION INTO A DETECTOR FROM A TILTED OCEAN WAVE FACET A-1

APPENDIX B LIST OF SYMBOLS B-1

FIGURES

1. Theoretical spectral radiance predicted by the Planck equation over π for ideal blackbodies of 6000 K (the red line, approximating the sun) and 300 K (the blue line, approximating the sea and sky) 5

2. Schematic representation of the maritime contributions to LOWTRAN 9

3. The geometry of reflection from a tilted wave facet on the ocean surface 13

4. Nondirectional wave slope probability as a function of solar zenith angle for a horizontal outlook centered on a glint pattern. Probabilities in the shaded area do not substantially contribute to the radiance 17

5. Nondirectional probability as a function of camera azimuth for a solar elevation of 10°. The camera is viewing the horizon, and the pattern is symetrical about the vertical axis 18

6. Nondirectional wave slope probability as a function of camera azimuth for a solar elevation of 20° 18

7. Nondirectional wave slope probability as a function of camera azimuth for a solar elevation of 30° 19

8. Nondirectional wave slope probability as a function of camera azimuth for a solar elevation of 40° 19

9. The Saunders shadowing factor as a function of the wind speed and zenith angle of the outgoing (camera) ray 20

10. The reflectivity of sea water as a function of optical wavelength for various solar zenith angles. The view is horizontal along the center of the glint pattern 22

11. The spectral irradiance for solar radiation incident on the ocean wave facet at 1450 PDT on 10 October 1991. The shaded area is 6.889 x 10^{-4} W cm^{-2} 22

12. Observed and calculated 3- to 5-μm radiance values for 0936 PDT on 14 March 1991. The horizontal line at 90.15° divides the data into those from the sky (above the line) and from the sea (below the line) 24

13. Calculated and measured radiance values in the 3- to 5-μm band on 26 July 1990 before solar glints were visible in the camera field of view 25

14. Calculated and measured values in the 3- to 5-μm band on 25 July 1990 when strong visible glint effects were filling the camera field of view. There is no Cox–Munk contribution 25

15. Calculated and measured radiance values on 10 October 1991 in the 3- to 5-μm band before solar glints were evident in the visible spectral region 27

16. Calculated and measured radiance values on 10 October 1991 in the 3- to 5-μm band. The fall off in the measured data is due to the Pt. Loma kelp beds 27

17. The data (dots) and total radiance (solid line) of figure 16 showing the effects of glint removal (dashed line) and a constant shift (dotted line) 28

INTRODUCTION

In the visible wavelength range, nighttime visibility is poor because the primary source of radiation, the sun, is hidden. However, because ordinary objects on the surface of the earth also radiate energy both day and night (albeit in the near- and mid-infrared ranges), it is possible to see at night through the eyes of an infrared camera. The spectral radiance (mW cm^{-2} str^{-1} μm^{-1}) of a 300-K blackbody is shown in figure 1, where it is compared with the spectral radiance of a 6000-K blackbody, which is a fair approximation to the solar spectral radiance.

It is an ironic fact that the *departure* of the earth's atmosphere from the 300-K blackbody law makes infrared vision possible. This is because the atmosphere of the earth (as well as the surface of the earth and the surface of the ocean) has radiances that approach the radiance of a 300-K blackbody, but only at those wavelengths where the radiances absorb strongly. Both the earth and ocean absorb strongly in the near-infrared, so their radiances are well approximated at their respective temperatures near 300 K by the blackbody function. The atmosphere contains two regions from approximately 3 to 5 microns and again from approximately 8 to 14 microns where absorption is low, especially for paths with small optical depths; for example, absorption is low directly up toward the zenith or horizontally from a high mountain range to deep space (Bell et al., 1960). In these spectral regions, the radiance of the atmosphere drops below the blackbody value. This is fortunate, however, because then the earth or sea (or a ship) can be seen through the relatively transparent atmosphere. Outside these regions, infrared eyes are blinded in the imediate vicinity of the camera by the blackbody radiance of the atmosphere. The transparency of the atmosphere in these spectral regions in the mid- and far-infrared, together with recent advances in infrared detector technology, make knowledge of the infrared radiance and transmission in the vicinity of the earth important to the armed services. This knowledge affects the services' ability to operate at night almost as well as they can operate during the day.

This document concerns radiance models that can be used to predict the infrared behavior of the sea, land, and sky. Personnel can compare the predicted behavior with experiments.

MARINE MODIFICATION OF LOWTRAN 6

The Atmospheric Transmittance/Radiance Computer Code LOWTRAN 6 (Kneizys, et al., 1983) has recently been modified by Wollenweber (1988), who introduced radiance reflections and blackbody emissions from the sea surface into the code sky in order to provide a more realistic representation of the infrared marine environment. In this report, we describe the inclusion of an additional contribution that is also important in marine settings: sun glint, which is the specular reflection of solar rays into an infrared camera by the ocean surface.

The general idea of the maritime modification of the LOWTRAN 6 computer code is presented in figure 2. The camera, located a short distance above the ocean surface typical of shipboard heights (e.g., 30 m), is adjusted to view the sky and sea in the vicinity of the horizon, so its zenith angle usually falls within a degree or so of 90 degrees. The horizontal range will be on the order of a few tens of km at an altitude of 30 m. Since typical instantaneous fields of view for infrared cameras are on the order of 1 mrad, the linear dimensions of a single camera pixel at the ocean surface—the pixel footprint—will be a few tens of m.

The footprint of a single pixel is shown schematically in figure 2. Prior to the work of Wollenweber (1988), LOWTRAN 6 calculated the radiance along the atmospheric path from the

camera to the footprint. This atmospheric path is labeled "path radiance" in figure 2. This calculated radiance was taken as the total radiance reaching the camera. Infrared radiance measurements of the sea and sky in the vicinity of the ocean horizon, however, often resulted in larger radiances than those predicted by LOWTRAN 6, pointing out the need for additional radiance mechanisms in such a setting.

Two additional radiance contributions introduced by Wollenweber (1988) can be understood as follows. The pixel footprint will contain numerous individual wave facets, each one perhaps a mm or less in extent and each one with its own orientation, which constantly changes with time as the wind ruffles the open sea surface. Within the footprint, a facet with a given instantaneous slope will reflect a portion of the sky dome into the camera. This radiance is labeled "sky dome radiance" in figure 2. Furthermore, the ocean itself radiates like a blackbody at the temperature of the water, so each facet will emit blackbody radiation into the sky dome above it and some of the radiation will enter the camera. This radiance is labeled "emissions" in figure 2. These two additional sources of infrared radiance were added to the LOWTRAN 6 computer code by Wollenweber in 1988. Richter, Hughes, and Paulson (1989) showed that these maritime additions to LOWTRAN 6 substantially increased the agreement between predicted and observed radiances near the sea horizon in the 8- to 12-micron spectral region.

At this point, we should note that in this wavelength band (8 to 12 microns), observations have shown that glitter is not a significant source of radiance. Since 1989, however, rapid strides in detector technology in the 3- to 5-micron spectral region have intensified interest in this spectral band and, here, sun glint is known to make a major contribution. This could have been expected from figure 1, which shows two trends occurring when spectral radiance moves from the middle of the 8- to 12-micron band (say 10 microns) to the middle of the 3- to 5-micron band (say 4 microns): First, the solar spectral radiance *rises* by more than an order of magnitude (the actual ratio is 33) in going from 10 to 4 μm and, second, the 300-K spectral radiance *falls* by more than an order of magnitude (the actual ratio is 15) in going from 10 to 4 μm. Hughes (1992) showed that even with the two Wollenweber additions for reflected sky radiance and sea surface emissions, the model predictions fall short of the sea radiances observed in the presence of sun glint (1992a).

SUN GLINT

This work was undertaken following the suggestion of Hughes that sun glint be included in the maritime modifications to LOWTRAN 6 (1992a). Some indication of the importance of solar reflections to infrared shipboard receivers can be obtained from the following statement: "Shipboard defense systems employing infrared warning receivers have experienced saturation of threat detection processing circuits due to the signal resulting from solar reflection (glints) from the rough sea surface. . . ." The analysis shows that the use of a linear polarizer with a shipboard IR warning receiver can typically be expected to increase the number of daylight hours that the sensor can be operated without any blanking, and to narrow the azimuth sector for which blanking is required for low sun angles. . . . With a linear polarizer the number of hours for which blanking will be necessary can typically be reduced to 6 to 8 hours per day and the azimuthal extent of the blanking during the remaining hours reduced to ± 12°" (Beard, 1976, p. 5).

The seminal paper on sun glint, or glitter as it is sometimes called, is by Cox and Munk (1954). This paper remains definitive to this day. The equations and results of Cox and Munk

together with the calculations available within the LOWTRAN 6 code will be the basis of the work presented here.

The glint has been included according to the following approach. For a perfectly calm sea, the entire pixel footprint will reflect the sun's rays into a properly oriented camera. An equation given by Cox and Munk (1954) can be used to relate the solar spectral irradiance (W cm^{-2} μm^{-1}) falling on the sea to the spectral radiance (W cm^{-2} str^{-1} μm^{-1}) leaving the sea. When multiplied by the spectral extinction transmittance along the entire path from footprint to camera, this radiance is the sun glint contribution we are seeking.

In reality, however, only a certain fraction of the facets will be correctly positioned within the footprint to let a mirror-like specular reflection of the sun's rays into the camera. Given the position of the camera and the sun, it is a simple matter of geometry to calculate the facet slope required for a specular reflection. Cox and Munk (1954) show that once the wind velocity is known, the fraction of facets whose slopes lie near a given value can be calculated. This spatial fraction, which can also be regarded as a temporal probability function, is then applied to the radiance described above in order to provide a more realistic representation of the sun glint radiance reaching the camera. This contribution is labeled "solar irradiance" in figure 2.

Figure 1 (overleaf). Theoretical spectral radiance predicted by the Planck equation over p for ideal blackbodies of 6000 K (the red line, approximating the sun) and 300 K (the blue line, approximating the sea and sky). The blue dashed line is a nominal value for the radiance of the sky produced by diffusely scattered sunlight. The combined effect of scattered sunlight and radiation emitted from the atmosphere at the earth's temperature can be estimated by adding the two blue curves, and in many situations this comes close to the actual spectral radiance of the daytime sky (Bell et al., 1960).

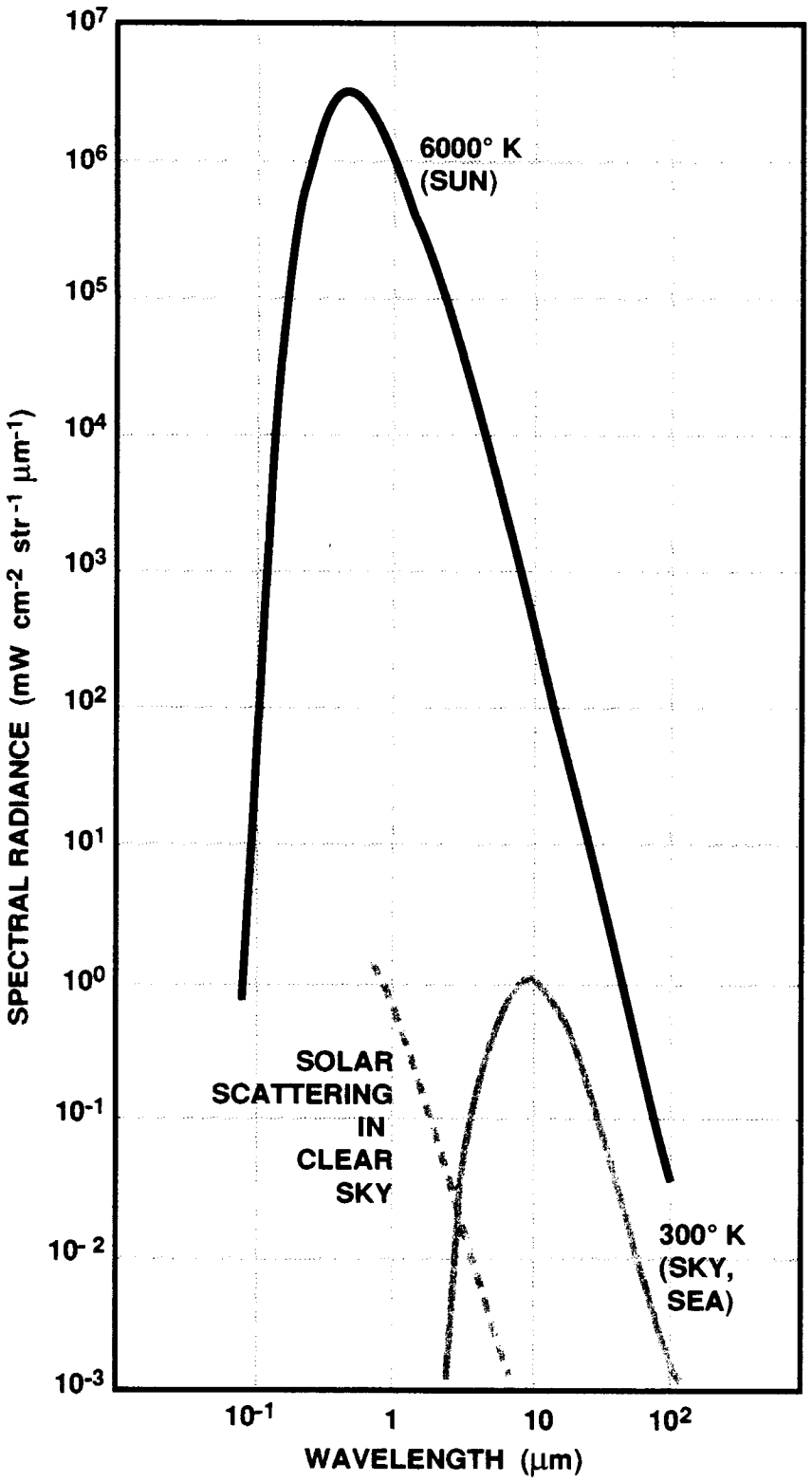
SPECTRAL RADIANCE (mW cm-2 str-1 μm-1)
10^7
10^6
10^5
10^4
10^3
10^2
10^1
10^0
10^-1
10^-2
10^-3
6000° K
(SUN)
SOLAR
SCATTERING
IN
CLEAR
SKY
300° K
(SKY,
SEA)
10^-1
1
10
10^2
WAVELENGTH (μm)

Figure 2 (overleaf). Schematic representation of the maritime contributions to LOWTRAN. The infrared camera, typically located on board ship, produces a picture consisting of a sequence of picture resolution elements, or pixels. The pixel footprint, typically 10 m on a side, consists of that portion of the ocean whose radiance contributes to the formulation of a single pixel. Unmodified LOWTRAN calculates the radiance along the path from the camera to the pixel footprint ("path radiance"). The marine modifications take into account the following additional contributions: blackbody radiation from the sea itself ("emissions"); the radiance from the entire sky hemisphere reflected in the surface of the sea ("sky dome radiance"); and reflected solar irradiance, or sun glint ("solar irradiance").

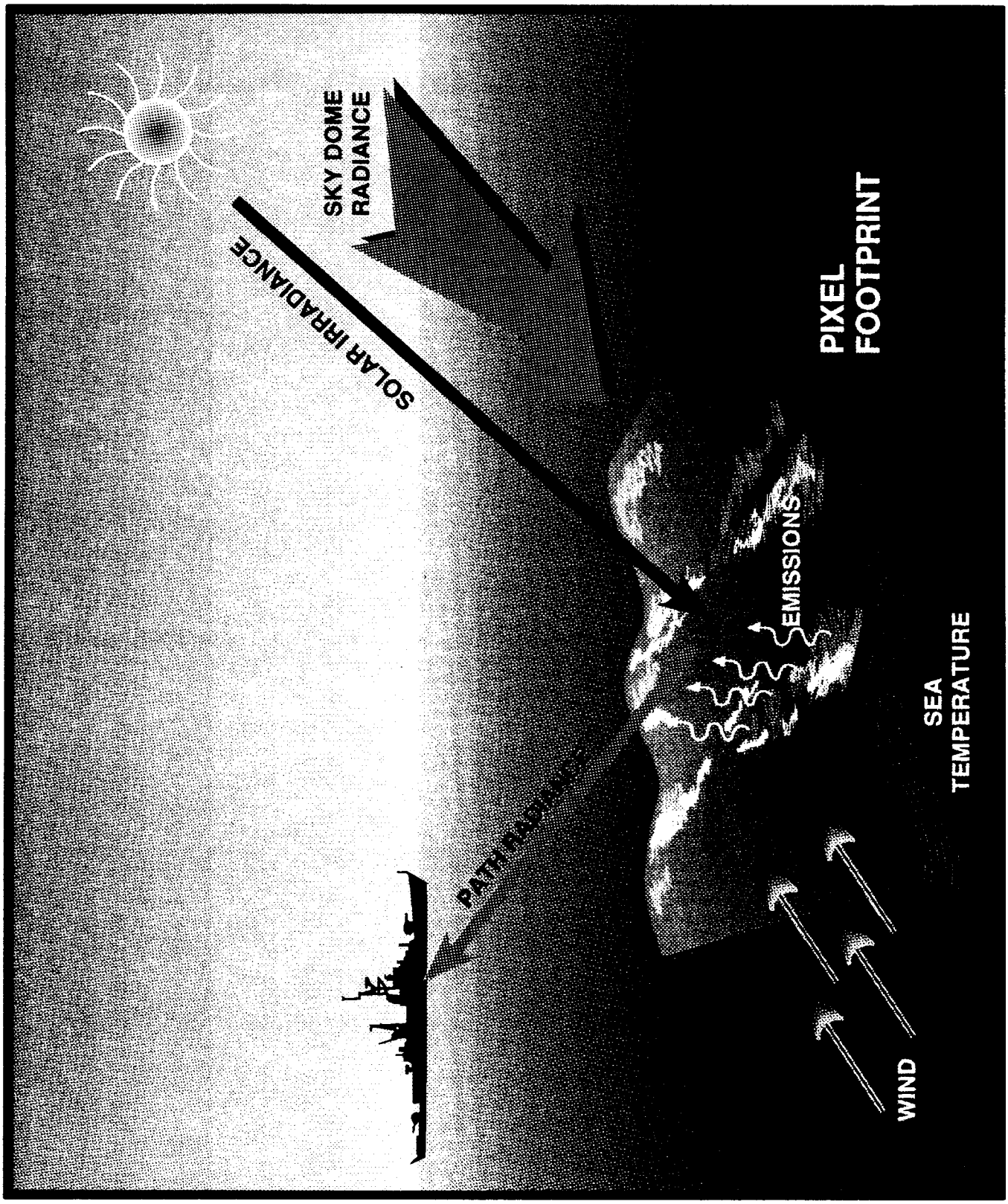
SKY DOME
RADIANCE
SOLAR IRRADIANCE
PATH RADIANCE
EMISSIONS
PIXEL
FOOTPRINT
SEA
TEMPERATURE
WIND

SUN GLINT FORMULATION

The geometry of the point of reflection is shown in figure 3. The coordinate system, its orientation, and the meaning of all the angles are discussed in detail in appendix A.

If the instantaneous slope of a facet in the upwind direction is $\tan\alpha$, and if the instantaneous slope of the facet in the crosswind direction is $\tan\beta$, then let the fraction of facets whose slopes lie within $\pm(d\tan\alpha)/2$ of $\tan\alpha$ and $\pm(d\tan\beta)/2$ of $\tan\beta$ be given by the probability function

$$p(\tan\alpha, \tan\beta, W)\, d\tan\alpha\, d\tan\beta \ , \tag{1}$$

where it has been anticipated that the probability will depend on the wind velocity **W** (ms^{-1}).

If the spectral solar irradiance H_λ^{facet} ($W\ cm^{-2}\ \mu m^{-1}$) falling on the facet can be found, then the spectral radiance N_λ^{facet} ($W\ cm^{-2}\ str^{-1}\ \mu m^{-1}$) leaving the facet can be calculated from the following formula originally given by Cox and Munk (1954) and later adapted for use near the horizon by Saunders (1968):

$$N_\lambda^{facet} = \frac{p(\tan\alpha, \tan\beta, W)}{4\cos^4\gamma} \cdot \frac{S(\theta, W)}{\cos(\theta)} \cdot R(\Omega, \lambda) \cdot H_\lambda^{facet} . \tag{2}$$

Here, R is the reflectivity of the facet, Ω is the angle of incidence, λ is the wavelength, γ is the facet tilt, θ is the zenith angle of the reflected ray,[1] and S is the Saunders shadowing factor. The radiance N_λ^{facet} leaving the facet must be multiplied by the spectral extinction transmittance $\tau_e(\lambda)$ along the entire path between the facet and the camera and integrated over the spectral band to obtain the final result for the contribution of the glint N, to the total radiance ($W\ cm^{-2}\ str^{-1}$) reaching the camera:

$$N = \int_{\lambda_1}^{\lambda_2} N_\lambda^{facet} \tau_e(\lambda) d\lambda \ . \tag{3}$$

[1]If refraction is neglected, angle τ is 180° minus the zenith angle of the camera.

Figure 3 (overleaf). The geometry of reflection from a tilted wave facet on the ocean surface. The plane of incidence contains the incident ray, the facet normal (not shown), and the reflected ray. The x–y plane is horizontal and the x axis is chosen to point upwind. A full discussion of this geometry, including the meaning of the various angles, is given in the appendix.

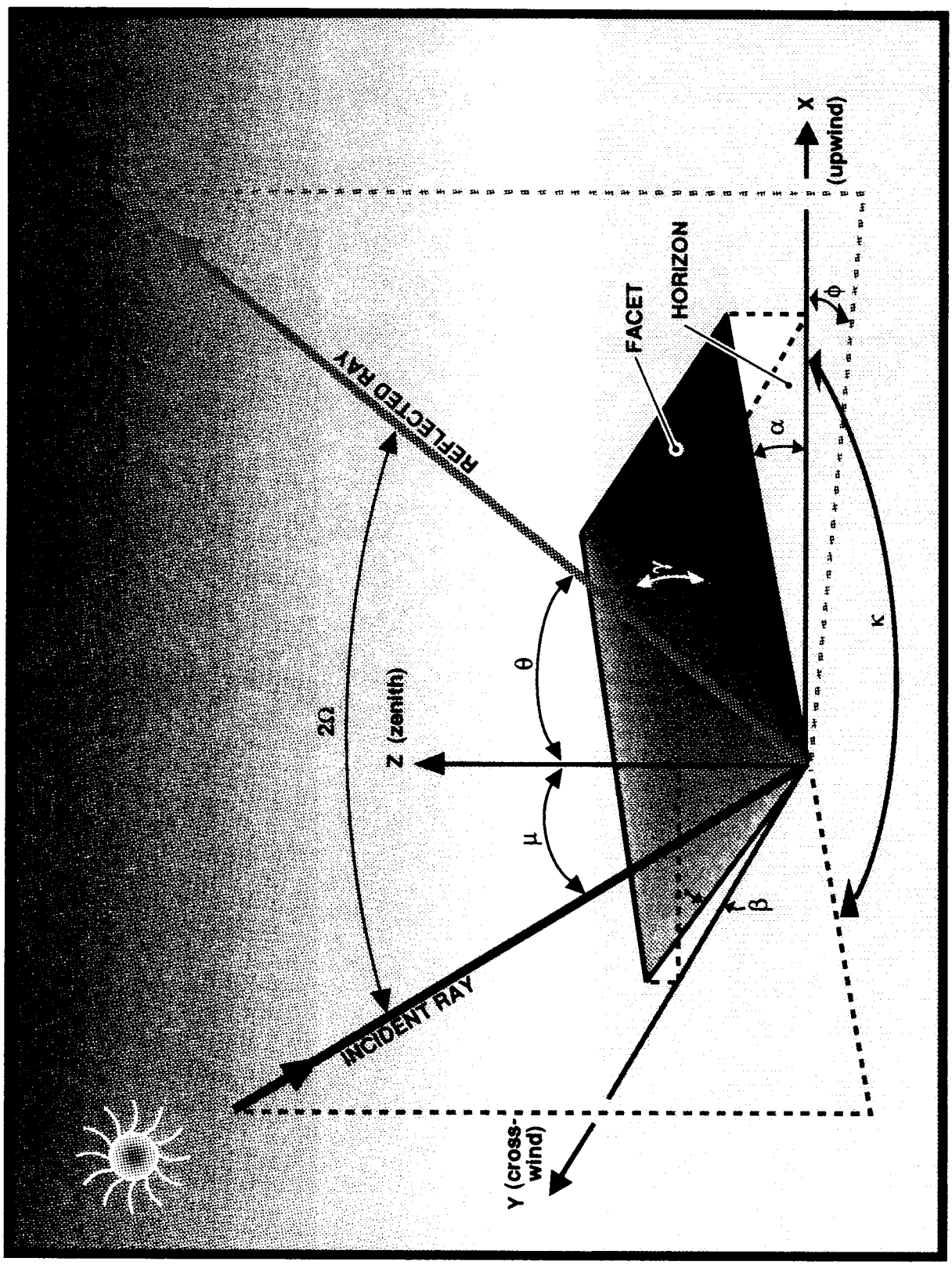
X
(upwind)
HORIZON
FACET
REFLECTED RAY
INCIDENT RAY
Z (zenith)
Y (cross-wind)
2Ω
θ
μ
α
β
γ
φ
κ

DETAILS OF THE FORMULATION

The following will explain how each term in equations (2) and (3) was obtained and provide examples of the terms' values that were appropriate to the situation obtained on 10 October 1991 at 1450 PDT (hereafter called "10 October") when sun glint data were taken at Point Loma in San Diego, CA.

Let azimuths ϱ be measured positive clockwise from true north when looking down and let $\varrho_{detector}$ be the azimuth of the direction in which the camera is pointing.

Wind velocity $\boldsymbol{W}$ is taken from measurements of wind speed and wind direction. The wind direction sets the orientation of the x axis and thereby determines the relative azimuths of the camera ($\varrho_{detector} - \varrho_{wind} \equiv \phi + \pi$) and the sun ($\varrho_{source} - \varrho_{wind} \equiv \varkappa$), with respect to the wind (see appendix A).

The facet slopes, $\tan\alpha$ and $\tan\beta$, and the cosine of the angle of incidence, Ω, are calculated from the following equations whose derivation is given in appendix A:

$$\tan\alpha = (-\sin\theta\cos\phi - \sin\mu\cos\varkappa)/(\cos\theta + \cos\mu)$$

$$\tan\beta = (+\sin\theta\sin\phi + \sin\mu\sin\varkappa)/(\cos\theta + \cos\mu) \qquad (4)$$

$$\cos\Omega = [(1 + \sin\theta\cos\phi\sin\mu\cos\varkappa + \sin\theta\sin\phi\sin\mu\sin\varkappa + \cos\theta\cos\mu)/2]^{1/2}$$

On 10 October, the wind speed was westerly ($\varrho_{wind} = 90°$) at 4.6 m s^{-1}; the camera was centered on the horizon ($\theta = 90°$) pointing south southwest ($\varrho_{wind} = 225°$); and at 1450 PDT the solar zenith angle μ was 50.47° at an azimuth ϱ_{source} of 224.79°. With these values, equation (4) gives 14.3° for α, -14.3° for β, and 70.2° for Ω.

It is easy to show from the equations given by Cox and Munk (1954) that the tilt (γ, the angle between the horizon and the direction of steepest ascent within the facet) is related to the x and y slopes by

$$\tan^2\gamma = \tan^2\alpha + \tan^2\beta \ . \qquad (5)$$

On 10 October, the tilt was 19.8°.

Cox and Munk (1954) determined $p(\tan\alpha, \tan\beta, W)$ for the ocean surface by means of airborne photographic measurements. They found that

$$p(\tan\alpha, \tan\beta, W) = (2\pi\sigma_u\sigma_c)^{-1} \exp - \frac{1}{2}\left(\frac{\tan^2\alpha}{\sigma_u^2} + \frac{\tan^2\beta}{\sigma_c^2}\right)$$

$$\sigma_u^2 = 0.000 + 3.16 \cdot 10^{-3}W \tag{6}$$

$$\sigma_c^2 = 0.003 + 1.92 \cdot 10^{-3}W$$

where σ_u and σ_c are the standard deviations in the upwind (x) and crosswind (y) directions, respectively. Both depend on the wind speed, which must be entered into these expressions in ms^{-1}. A wind speed of 1 ms^{-1} is typical of a calm sea; a wind speed of 10 ms^{-1} is typical of a rough sea.

For a particular wind speed, the value of p in equation (6) will oscillate up and down about an average value q given by equation (6), with σ_u^2 and σ_c^2 each replaced by its average value $\sigma_{av}^2 = (\sigma_u^2 + \sigma_c^2)/2$:

$$q(\tan\gamma, W) = (2\pi\sigma_{av}^2)^{-1} \exp - \frac{1}{2}\left(\frac{\tan^2\gamma}{\sigma_{av}^2}\right)$$

$$\sigma_{av}^2 = 0.0015 + 2.54 \cdot 10^{-3}W \tag{7}$$

We shall call q the nondirectional wave slope probability.

Of all the factors in equation (2), p is the most rapidly varying function of geometry and meteorology. For most cases of interest, p falls within about a factor of 2 of q, whereas q itself varies between 100 and 0.01. Therefore, the value of N_λ^{facet} can be estimated by inspecting the value of q; in the 3- to 5-micron region, a nondirectional probability of 0.1 or more is required for sun glint to make a significant contribution (0.1 °C or more) to the observed radiance. Figure 4 shows how q varies with solar zenith angle (or, equivalently, solar elevation) for the case of a horizontal view ($\theta = 90°$) down the center of a glint pattern toward the sun ($\varrho_{detector} = \varrho_{source}$). The following four figures (figures 5–8) show the value of q as the camera moves off the center of the glint pattern. Figures 5 to 8 refer to a fixed solar zenith angle with the camera viewing horizontally at various wind speeds. Figure 8 ($\mu = 50°$), displaying a wind speed of 5 ms^{-1} for 10 October, shows that q was in the vicinity of 0.1.

The shadowing factor was introduced by Saunders (1968) to account for the fact that one facet can hide another when the sea surface is viewed at very shallow glancing angles on the far horizon. Further motivation for this factor was the unbounded nature of equation (2), absent S, near the horizon—that is for $\cos(\theta)$ in the denominator of equation (2) approaching zero. "Without the inclusion of shadowing, we find that when [$\cos(\theta)$] becomes very small, the radiance calculated from equation (2) becomes unbounded; by including S, which goes to zero with [$\cos(\theta)$] we ensure that the radiance calculated from equation (2) remains finite" (Saunders, 1968, p. 648). Saunders' shadowing factor is

$$
\begin{aligned}
S(\theta, W) &= 2[1 + erf(\nu) + (\nu\sqrt{\pi})^{-1}\exp(-\nu^2)]^{-1} \\
\nu &= \frac{\tan(\pi/2 - \theta)}{\sigma} \\
\sigma^2 &= 2\sigma_{av} = \sigma_u^2 + \sigma_c^2 \\
&= 0.003 + 5.12 \cdot 10^{-3} W ,
\end{aligned}
\tag{8}
$$

where *erf(v)* is the error function. Figure 9 gives the value of the ratio $S(\theta, W)/\cos(\theta)$ for various wind speeds. Within a degree of the horizon, this ratio is approximately 20 for a wind speed of 5 ms^{-1}, which was the approximate value on 10 October.

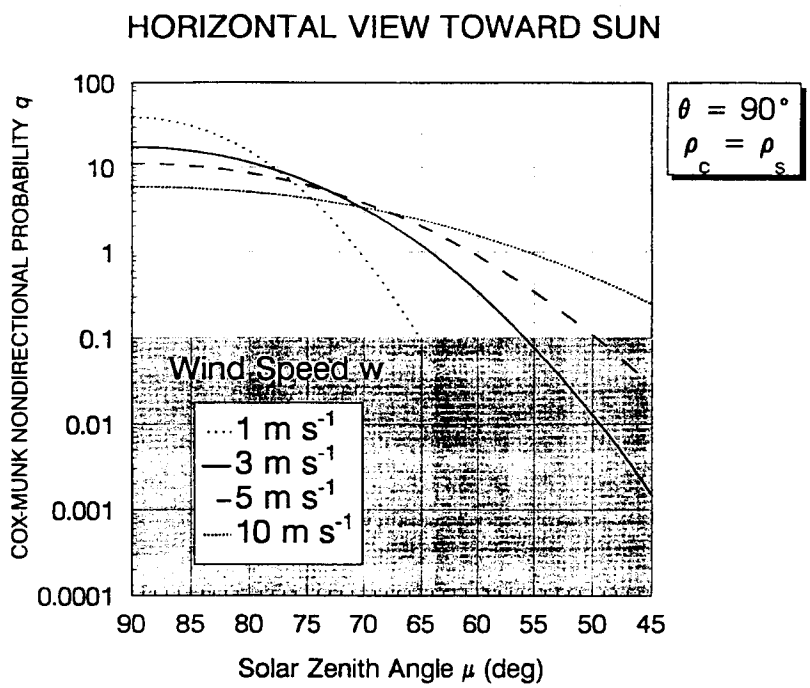

Figure 4. Nondirectional wave slope probability as a function of solar zenith angle for a horizontal outlook centered on a glint pattern. Probabilities in the shaded area do not substantially contribute to the radiance.

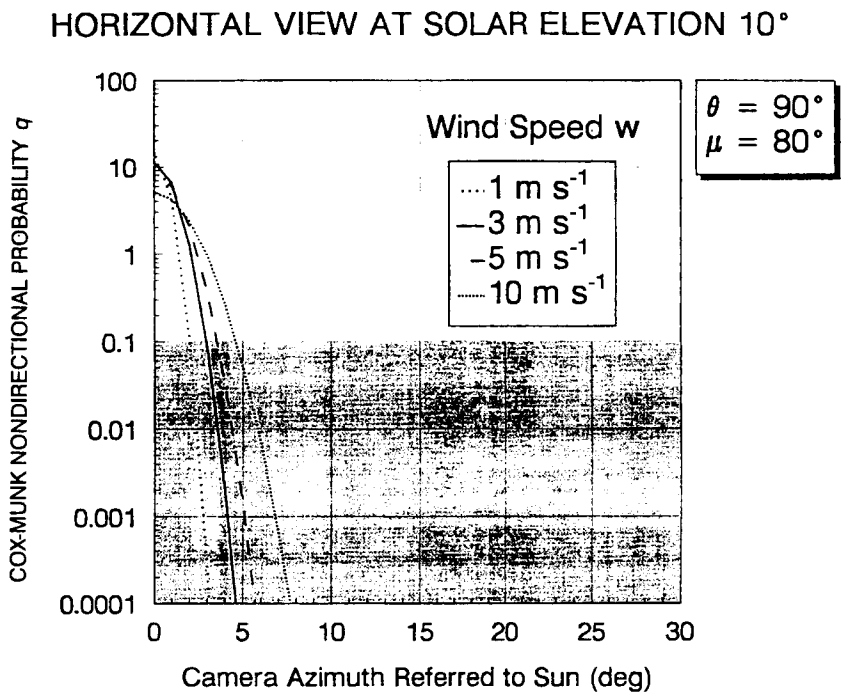

Figure 5. Nondirectional probability as a function of camera azimuth for a solar elevation of 10°. The camera is viewing the horizon and the pattern is symetrical about the vertical axis.

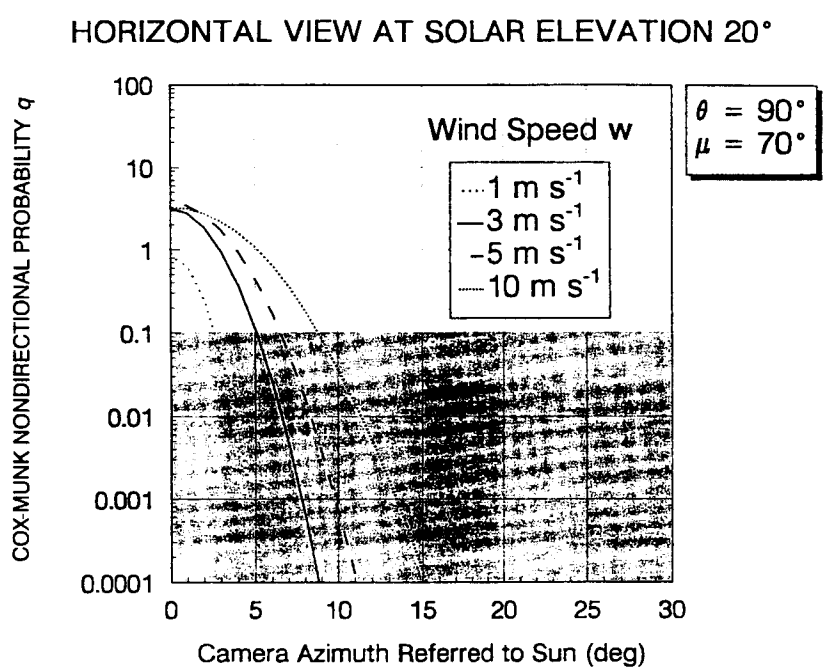

Figure 6. Nondirectional wave slope probability as a function of camera azimuth for a solar elevation of 20°.

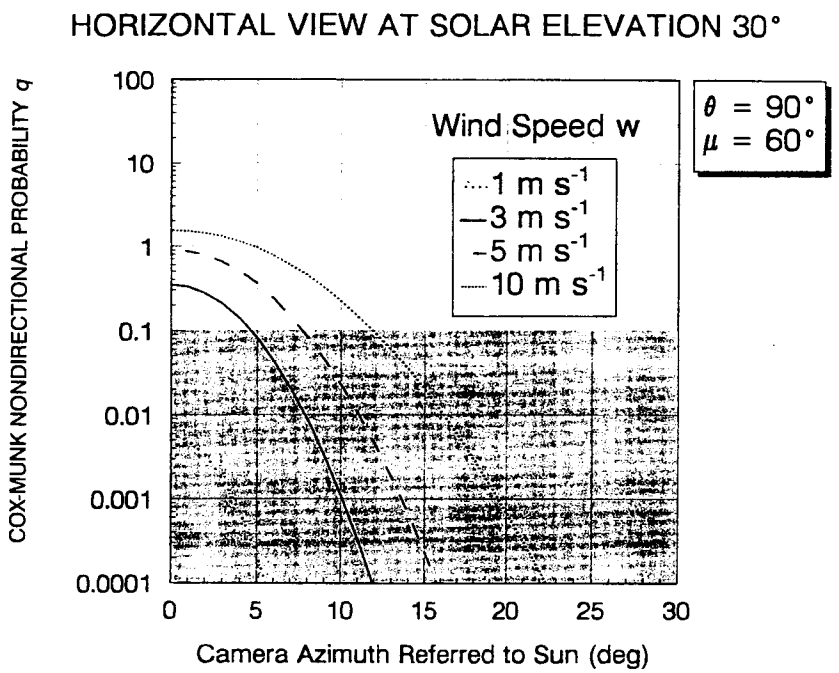

Figure 7. Nondirectional wave slope probability as a function of camera azimuth for a solar elevation of 30°.

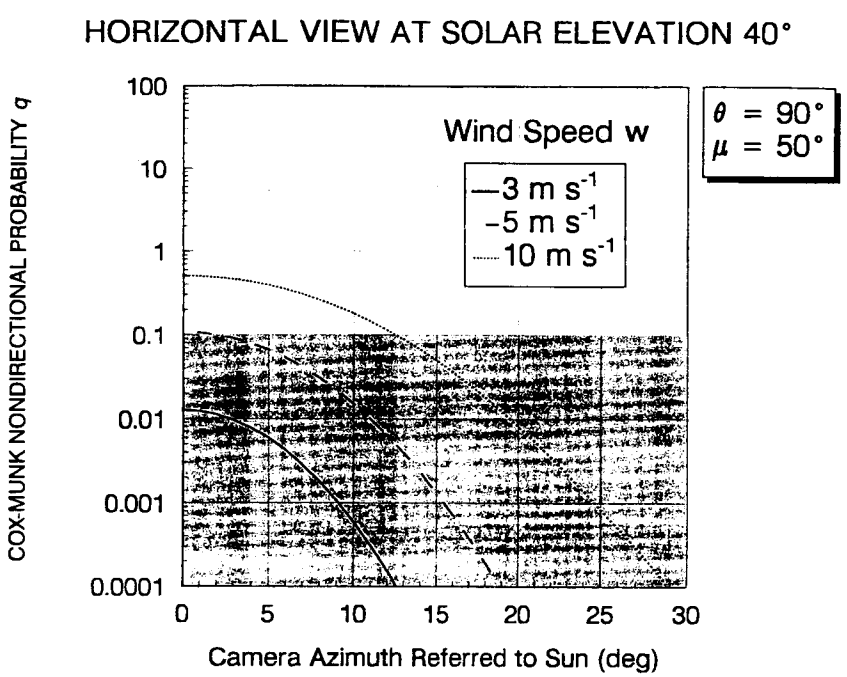

Figure 8. Nondirectional wave slope probability as a function of camera azimuth for a solar elevation of 40°.

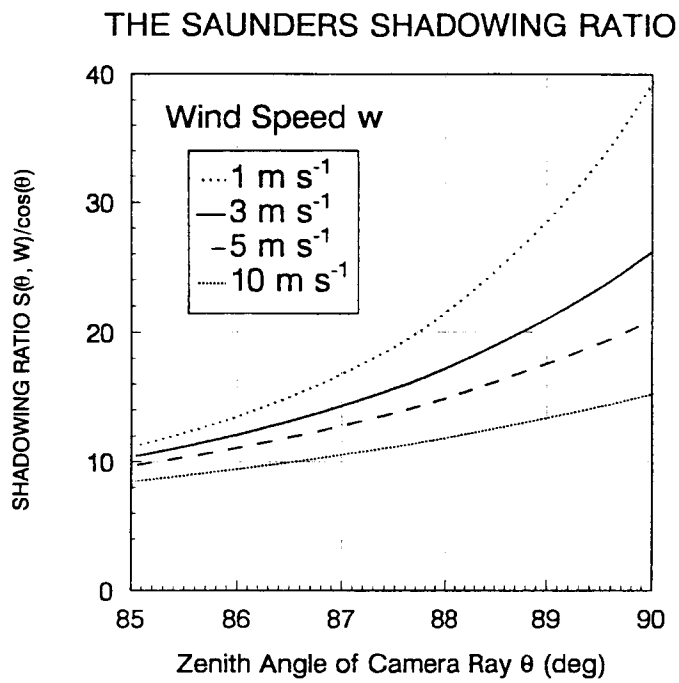

Figure 9. The Saunders shadowing factor as a function of the wind speed and zenith angle of the outgoing (camera) ray.

The reflectivity of the sea water facet $R(\Omega, \lambda)$ is given by Fresnel's equations governing the reflection of unpolarized light by a nonmagnetic conducting medium with a complex refractive index $\alpha(\lambda) + i\beta(\lambda)$ (Stratton, 1941; pp. 505, 506; eqs 74, 77):

$$
\begin{aligned}
R(\Omega,\lambda) &= (R_p + R_s)/2 \\
R_p &= \frac{(q - \cos\Omega)^2 + p^2}{(q + \cos\Omega)^2 + p^2} \\
R_s &= \frac{([\alpha^2 - \beta^2]\cos\Omega - q)^2 + (2\alpha\beta\cos\Omega - p)^2}{([\alpha^2 - \beta^2]\cos\Omega + q)^2 + (2\alpha\beta\cos\Omega + p)^2} \\
q^2 &= (\ + g + \sqrt{h^2 + g^2})/2 \qquad (9) \\
p^2 &= (\ - g + \sqrt{h^2 + g^2})/2 \\
g &= \alpha^2 - \beta^2 - \sin^2\Omega \\
h &= 2\alpha\beta \ .
\end{aligned}
$$

The index for sea water between 3 and 28 μm was taken from literature (Hale and Querry, 1973; Querry et al., 1977). Figure 10 gives the value of the reflectivity of sea water along the center of a glint pattern as a function of wavelength for a variety of solar elevations; the reflectivity was between 10% and 15% for 10 October.

The spectral extinction transmittance and the spectral solar irradiance (figure 11) reaching the facet were obtained from LOWTRAN.

FORTRAN CODING

The preceding equations were introduced into the LOWTRAN 6 FORTRAN computer code along lines established by Wollenweber (1988). For those familiar with LOWTRAN, a brief summary of Wollenweber's approach is now given.

LOWTRAN calculates radiance while tracing a ray backwards from the detector toward the edge of the atmosphere. If the ray remains in the atmosphere, then no alteration is made to the original radiance calculation and the result is the radiance of a pixel in the sky. If, on the other hand, the ray hits the lower boundary of the atmosphere, then this boundary is reinterpreted as the surface of the sea, the calculation is interrupted, and the radiance computed thus far is saved as the path radiance of figure 2. During the interruption, a Wollenweber subroutine called WAVE typically issues 8 to 12 new LOWTRAN-compatible "geometry cards" representing the sky dome. Each new card has height 0 and a zenith angle that the Cox–Munk wave slope statistics have determined contributes at least 5% to the overall sky radiance reaching the camera after reflection in the sea surface. (The geometry of this situation corresponds to the geometry of problem one in appendix A.) The calculation is then resumed to derive the radiance along each of the new sky dome paths. All sky dome radiances are reflected in the sea and added together to arrive at the contribution labeled "sky dome" in figure 2.

In addition, the geometry of the reflection is fully determined (problem one in appendix A again) for each new zenith angle that has been introduced, since the geometry of the camera ray is fixed beforehand. Hence, the angle of incidence is also known, and can be used to calculate the emissivity (1 minus the reflectivity) of the facet, thus arriving at the contribution labeled "emissions" in figure 2.

For the glint calculation, the mode is temporarily changed from "atmospheric radiance" (IEMSCT = 2) to "directly transmitted solar irradiance" (IEMSCT = 3), and a final new "geometry card" is issued from the WAVE compatible with the new solar irradiance mode. H_λ^{facet} is then obtained upon resumption of the interrupted LOWTRAN calculation. (The solar position has already been introduced by means of a new card [Card 2E] in the LOWTRAN input file.) With the source and detector positions fixed, the geometry of the reflection is once again determined (problem two in appendix A), and new subroutines carry out the remainder of the calculations required by equation (2) resulting in the glint contribution labeled "solar irradiance" in figure 2.

If the original ray has hit the lower boundary of the atmosphere, then the radiance contributions described in the preceding three paragraphs are added together and the result is the radiance of a pixel in the sea.

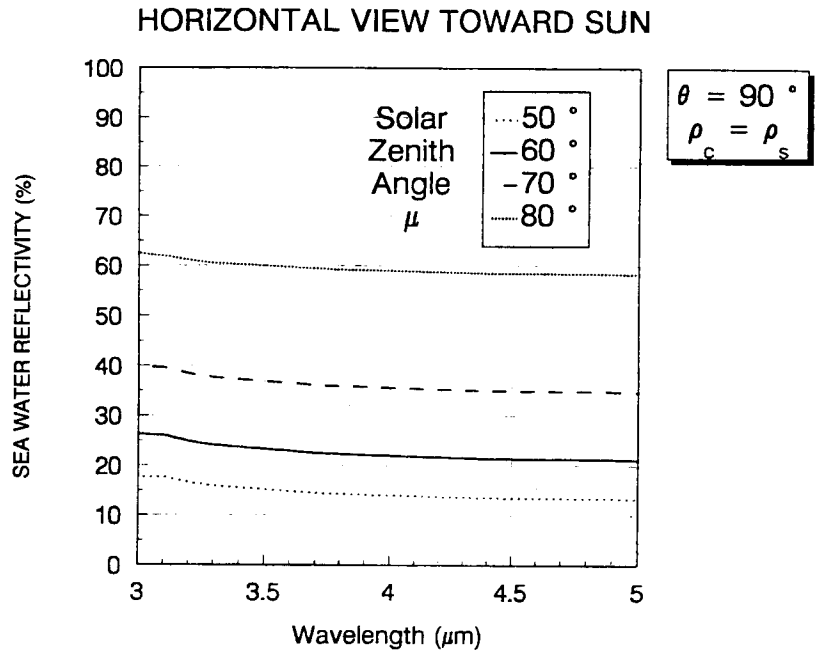

Figure 10. The reflectivity of sea water as a function of optical wavelength for various solar zenith angles. The view is horizontal along the center of the glint pattern.

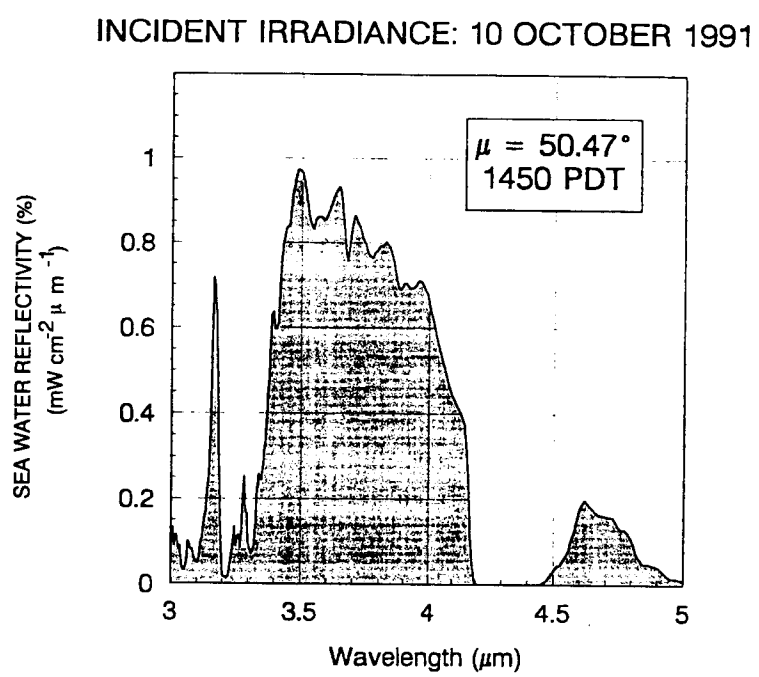

Figure 11. The spectral irradiance for solar radiation incident on the ocean wave facet at 1450 PDT on 10 October 1991. The shaded area is 6.889×10^{-4} W cm^{-2}.

Due to the general organization of LOWTRAN, equations such as (3) are not executed for the marine modifications. Equations similar to

$$N \approx \int_{\lambda_1}^{\lambda_2} N_{\lambda}^{facet}\, d\lambda \cdot \int_{\lambda_1}^{\lambda_2} \tau_e(\lambda) d\lambda \tag{10}$$

are executed instead. This is the Achilles heel of the marine modifications to LOWTRAN, because there is always the possibility that an unusual set of atmospheric conditions or ray parameters will cause a large error when we use this approximation. However, test cases show an error of 5% to 10% during its use under normal conditions.

COMPARISON WITH EXPERIMENT

Measurements of the near horizon radiance over the open ocean were made in the infrared at 3 to 5 μm and 8 to 12 μm by Hughes with a calibrated thermal imaging system (AGA THERMOVISION model 780) (1992b). The system has a 2.95° field of view and an instantaneous field of view of 0.87 mrad. Simultaneous measurements of meteorological parameters were acquired on the surface and with altitude by using balloon-borne radiosondes. Measurements were made on six different days, during which temperature inversions occurred at different heights. The surface winds were onshore in all cases (either northwesterly or westerly) at low to moderate speeds, the horizon was visible to the naked eye, and the cloud coverage did not exceed scattered conditions. The camera was set to a fixed position at a given altitude. As time passed, solar glints (if any) were brought into the camera's field of view. Three days have been selected to compare the calibrated thermal imaging system with LOWTRAN predictions. These days will be considered in order of the increasing importance of solar effects in the 3- to 5-μm band.

14 MARCH 1991

On 14 March 1991, data were taken at 0936 PST with the camera located at an altitude of 23 m and directed over the ocean on a bearing of 225°. The wind was westerly at 6.2 ms^{-1}. There was a high inversion level near 1900 m. This was in the morning, the solar azimuth was 129°, the solar zenith angle was 49°, and the effects of sun glint on the ocean surface were not noticeable. The measured 3- to 5-μm radiances are shown in figure 12, which is a vertical radiance slice consisting of a column of pixels taken from the full image. The box in the upper right-hand corner of the figure is a schematic representation of the azimuths of the wind (W), sun (S), and camera (C) at the time the data were taken. The small vertical arrow indicates true north. In the main part of the figure, the region above 90.15 represents the sky and the region below 90.15 represents the sea. On this day there was almost no difference between sea and sky radiances.

This raises the question of how the horizon is assigned in the infrared image. The assignment is made at a very distinctive cusp in the 8- to 12-μm data near the visible horizon, then retained for the 3- to 5-μm band. Furthermore, in the 8- to 12-μm band, the calculated radiance is forced

to match the measured radiance at the horizon by empirically adjusting the continental air mass factor (ICSTL in LOWTRAN) and the visibility (VIS in LOWTRAN). These parameters are then retained unchanged for calculations in the 3- to 5-μm band, where we generally discover that measured and calculated radiances obtained by these procedures do NOT agree. This disagreement will be much more evident in the subsequent figures.

The total radiance calculated for the sky and sea is shown after adjustment at the horizon according to the procedure of the previous paragraph by the solid line in figure 12. Although a close agreement between the calculation and the measurement appears at first, the discrepancy is actually large, on the order of 1°C—a value that should be compared to the measurement accuracy of several tenths of a degree C. The total computed radiance has been broken down in figure 12 into the path, sea, and sky contributions. There is no glint component, which is not surprising if we recall the conditions under which these data were taken. Without the marine modifications introduced by Wollenweber, the calculated radiance would follow the solid line in the sky and the dashed line in the sea. It is obvious that the modifications have moved the calculations much closer to the measurements. The same is true for all the following cases.

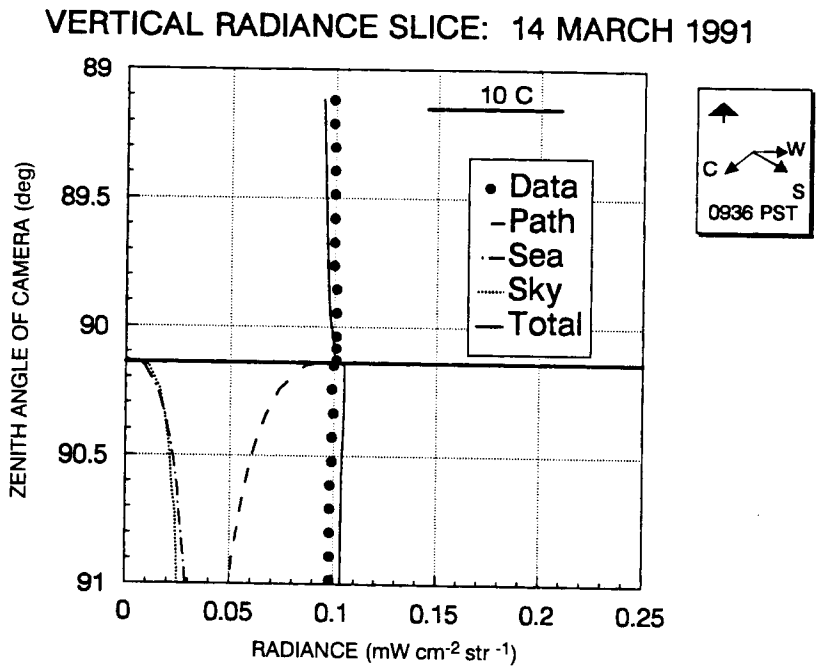

Figure 12. Observed and calculated 3- to 5-μm radiance values for 0936 PST on 14 March 1991. The horizontal line at 90.15° divides the data into those from the sky (above the line) and from the sea (below the line).

26 JULY 1990

The cameras were located at a 33-m altitude and pointed due west. The wind was out of the west at 1.8 m s^{-1} beneath scattered cumulus clouds. A strong temperature inversion near 400 m was recorded by the radiosonde launched at 1428 PDT. At 1536 PDT, the first data (figure 13) were taken, the solar azimuth and zenith angle were 259.4° and 37.9° respectivly, and no glint effects were observed visually. At 1613 PDT, the last data (figure 14) were taken, the solar azimuth and zenith angle were 265.6° and 45.6° respectively, and the 3- to 5-μm sensor was

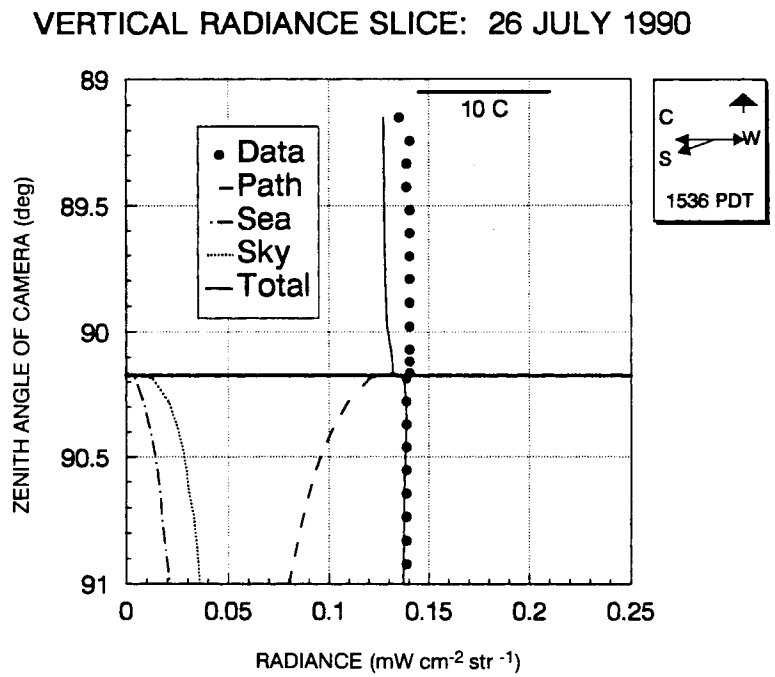

Figure 13. Calculated and measured radiance values in the 3- to 5-μm band on 26 July 1990 before solar glints were visible in the camera field of view.

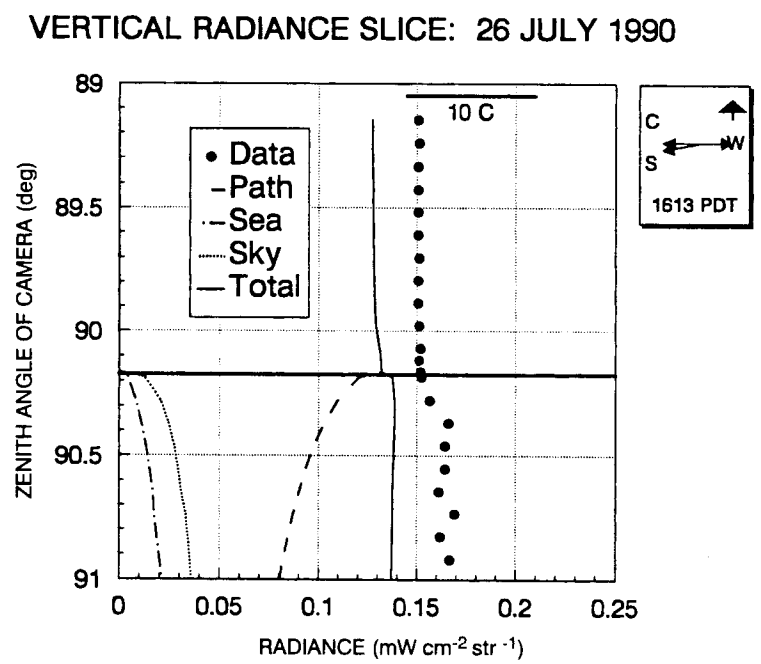

Figure 14. Calculated and measured radiance values in the 3- to 5-μm band on 26 July 1990 when strong visible glint effects were filling the camera field of view. There is no Cox–Munk contribution.

saturated as the visually observed glint filled the camera field of view. In the meantime, the 8- to 12-μm sensor did not saturate and remained unchanged between the first and last data. This agrees with expectations that solar glint effects should be much more prominent in the 3- to 5-μm band than in the 8- to 12-μm band.

What is surprising is that the Cox–Munk model shows *no* glint contribution for any of these 26 July data! In fact, at 1613, the calculated glint contribution was, at most, 5×10^{-9} W cm^{-2} str^{-1}. Apparently not enough facets were present with the slope required for a specular reflection. Figure 8 shows that even under the more favorable glint conditions of a 50° zenith angle and 3 ms^{-1} wind speed, the nondirectional wave slope probability is in the vicinity of 0.01, which is an order of magnitude too low for an observable contribution in the 3- to 5-μm band.

Without any glint contribution, the calculated radiance values are identical in figures 13 and 14, because they are based on the same atmospheric data and viewing geometry. Only the solar position has changed. Something indeed happened, however, because a large change occurred in the data measured between 1536 PDT and 1613 PDT: the sky radiance rose about 2°C and the sea radiance rose about 5°C. At this point, we must conclude that either the Cox–Munk model does not apply or that there is some other solar contribution we have yet to take into account.

10 OCTOBER 1991

The cameras were mounted at 23 m on a bearing of 225°. The day was very hazy without clouds. The wind was onshore at 4.6 m s^{-1}. A very strong temperature inversion began at the low altitude of about 60 m and ended at 428 m, where the temperature was 35°C. The first data were taken at 1153 PDT, and a second set were taken at 1240 PDT, when the sun's position was zenith angle 39.4° and azimuth 181°; visible sun glint effects began to appear at 1400 PDT, and the final data were taken at 1450 PDT as the glint pattern was exactly centered within the camera field (the solar position at 1450 was zenith angle 50.5°, azimuth 224.5°).

The measured data in figure 15 show a slight rise in the sky radiances compared to the sea radiances. This is a feature that Hughes attributed to the hot atmosphere close to the sea surface, which is due to the strong low inversion layer (1992b). The calculated and measured radiances match in the sea but not in the sky; the lack of a match in the sky has been encountered previously.

By 1450 PDT, both sea and sky radiances rose substantially and the sea radiance exceeded the sky radiance. (The drop in measured radiance between 90.6° and 91° occurred in the kelp beds about 1 km off the Point Loma shoreline; the ocean surface in these kelp beds is always smoother than the surface of the open sea, probably because of the effect of oil released by the kelp) (figure 16). The Cox–Munk model now makes a contribution to the radiance comparable to the sea emission and the reflected sky radiance. The total radiance matched the shape of the measured data (apart from the drop in the kelp beds), but a large offset of about 6°C took place in both sea and sky. In figure 17, the solid line labeled "shifted" was derived from the dotted line labeled "glint" by the arbitrary addition of 0.37 mW cm^{-2} str^{-1}. It can be seen that the shifted fit is extremely good outside the kelp beds. The glint is necessary for this fit: the dashed line in figure 17 shows what the total unshifted radiance would be without glint. It is interesting to note that a constant offset to the solid line of figure 14 would also produce a calculation running through the middle of the data. In this case, the offset would have a different value and the glint

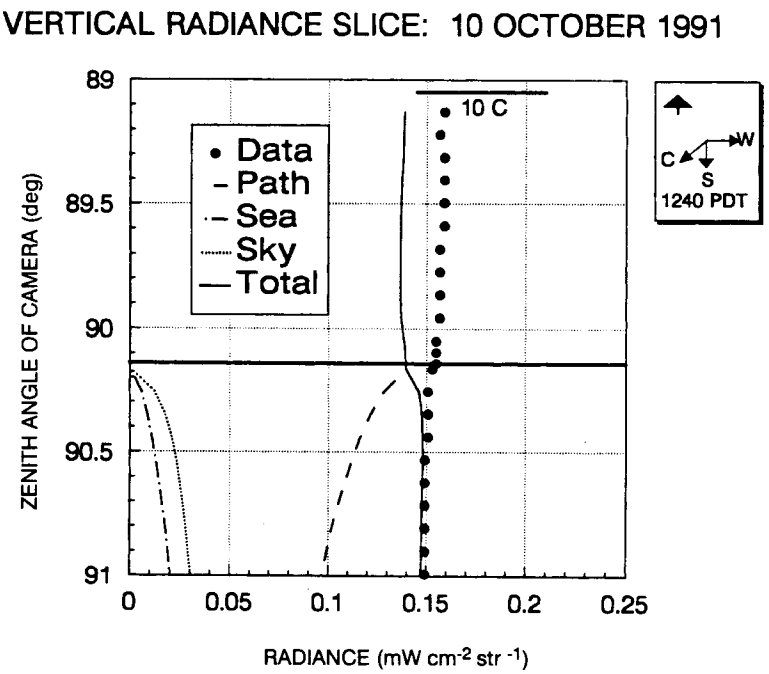

Figure 15. Calculated and measured radiance values on 10 October 1991 in the 3- to 5-μm band before solar glints were evident in the visible spectral region.

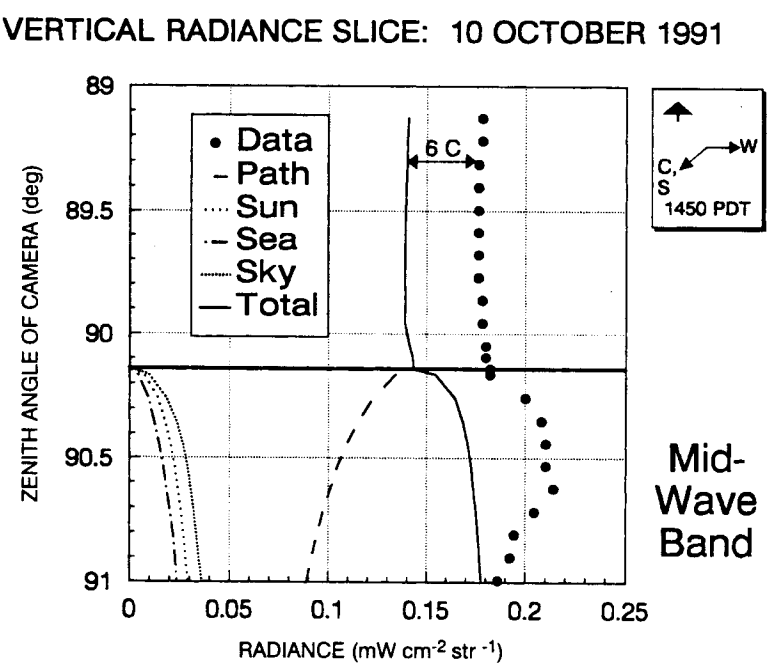

Figure 16. Calculated and measured radiance values on 10 October 1991 in the 3- to 5-μm band. The fall off in the measured data is due to the Pt. Loma kelp beds.

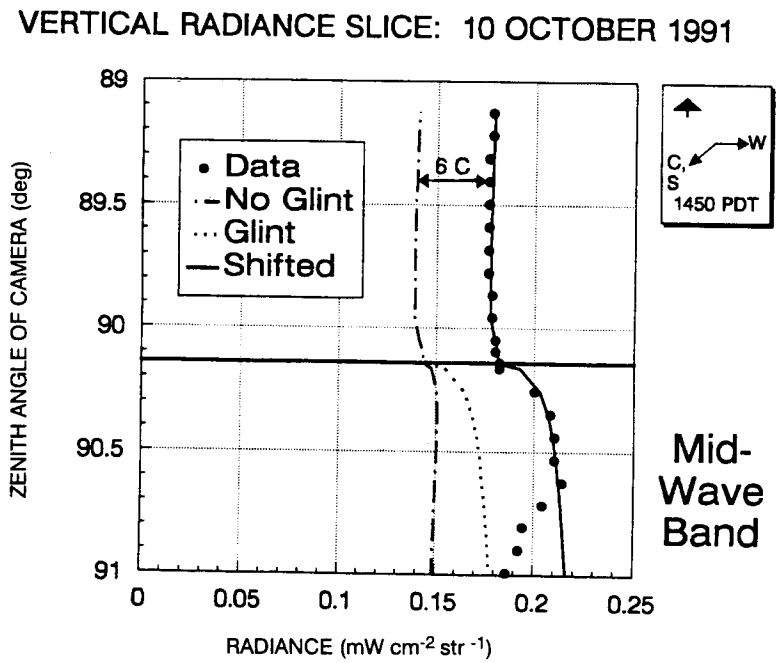

Figure 17. The data (dots) and total radiance (solid line) of figure 16 showing the effects of glint removal (dashed line) and a constant shift (dotted line).

would not be necessary for the fit. Judging from just these two days of data, an additional mechanism seems to exist creating a large increase in both sky and sea radiance at just the time when solar glitter (which of course affects the sea radiance alone) has its maximum impact. Such a mechanism might, for example, be multiple solar scattering, but it would have to enter into both sea and sky with equal strength, which appears to indicate that it must be independent of path length.

CONCLUSION

In this study, we have compared 3- to 5-μm radiance data measured over the open ocean (Hughes, 1992b) to the radiance predicted by the LOWTRAN 6 computer code (Kneizys et al., 1983), which was modified to take marine effects into account (Wollenweber, 1988). The marine effects are the following:

1. Blackbody emission from the sea.
2. Radiance from the sky reflected in the sea.
3. Solar reflection by the sea.

The data were taken with the intent of revealing radiance contributions due to the sun in the 3- to 5-μm band. We examined five sets of data on three different days and compared the data with the modified LOWTRAN 6 predictions.

We draw the following conclusions for the 3- to 5-μm band:

1. All of the marine modifications make an important improvement in the fit of the model to the data.
2. Significant discrepancies on the order of several degrees C remain between the model and the data.
3. Solar glints play a role but do not overwhelm (or even dominate) the data.
4. Another solar effect appears to play as strong a role as sun glitter. Its origin is unknown; we speculate that it may be multiple solar scattering.

REFERENCES

Beard, J. L. 1976. "Reduction of Solar Glints from the Sea with a Linear Polarizer," Technical Report 120500–9–T. Environmental Research Institute of Michigan, Ann Arbor, MI.

Bell, E. E., L. Eisner, J. Young,and R. A. Oetjen. 1960. "Spectral Radiance of Sky and Terrain at Wavelengths Between 1 and 20 Microns. II. Sky Measurements," *Journal of the Optical Society of America*, vol. 50, p. 1313.

Cox, C., and W. Munk. 1954. "Measurement of the Roughness of the Sea Surface from Photographs of the Sun's Glitter," *Journal of the Optical Society of America*, vol. 44, p. 838.

Hale, G. M., and M. R. Querry. 1973. "Optical Constants of Water in the 200 nm to 200 μm Wavelength Region," *Applied Optics*, vol. 12, p. 555.

Hughes, H. G. 1992a. "Sky and Sea Infrared Radiance Models: A Data Report of Measured Backgrounds and Meteorological Parameters," Naval Ocean Systems Center and Science and Technology Corporation, Hampton, VA.

Hughes, H. G. 1992b. "Sky and Sea Infrared Radiance Models: An Evaluation Report for the 3- to 5-mm and 8- to 12-μm Wavelength Bands," Technical Report 2574. Science and Technology Corporation, Hampton, VA.

Kneizys, F. X., E. P. Shettle, W. O. Gallery, J. H. Chetwynd, Jr., L. W. Abreu, J. E. Z. Selby, S. A. Clough, and R. W. Fenn. 1983. "Atmospheric Transmittance/Radiance: Computer Code LOWTRAN6," AFGL–TR–83–0187. Air Force Geophysics Laboratory, Hanscom Force Base, MA.

Querry, M. R., W. E. Holland, R. L. Waring, L. M. Earls, and M. D. Querry. 1977. "Relative Reflectance and Complex Refractive Index in the Infrared for Saline Environmental Waters," *Journal of Geophysical Research*, vol. 28, p. 1425.

Richter, J. H., H. G. Hughes, and M. R. Paulson. 1989. "Effect of Marine Atmosphere on Performance of Electro-Optical Systems," NOSC TD 1635. Naval Ocean Systems Center, San Diego, CA.

Saunders, P. M. 1968. "Radiance of Sea and Sky in the Infrared Window 800–1200 cm^{-1}," *Journal of the Optical Society of America*, vol. 58, pp. 645–648.

Stratton, J. A. 1941. *Electromagnetic Theory*, pp. 505–506. McGraw-Hill, New York, NY.

Wollenweber, F. G. 1988. "Infrared Sea-Radiance Modeling Using Lowtran 6," NOSC TD 1355. Naval Ocean Systems Center, San Diego, CA.

APPENDIX A

DERIVATION OF GEOMETRIC EQUATIONS GOVERNING THE REFLECTION OF RADIATION INTO A DETECTOR FROM A TILTED OCEAN WAVE FACET

THE GEOMETRY

The geometry at the point of reflection is shown in figure 3 in the main text (after Cox & Munk, 1954). The various quantities in figure 3 as well as others that will be required are defined by the following concepts:

The Coordinate System

Choose a coordinate system whose origin is the point of reflection. Let the x axis point upwind, the z axis toward the zenith, and the y axis crosswind such that a right-handed system is formed. The x–y plane is tangent to the earth (horizontal) at the point of reflection. Let azimuthal angles ϱ be measured in the x–y plane (the horizon) and consider them to be positive when measured clockwise from north looking down along the $-z$ direction. All azimuths point away from the origin except the azimuth of the detector, which points toward the origin along the line of detector sight.

The Tilted Facet

Let the tilted facet pass through the origin. Let $\tan\alpha$ be the facet slope dz/dx in the x–z plane, and let $\tan\beta$ be the facet slope dz/dy in the y–z plane. Define a unit vector $\boldsymbol{u_n}$ normal to the facet with components (a_n, b_n, c_n).

The Source

The incoming ray is bent due to the effects of refraction. At the point of reflection define μ to be the zenith angle of the ray arriving from the source or, in other words, the apparent angle from the zenith to the source regarded from the origin. Azimuthal angles are not affected by refraction. Let $\varkappa$ be the azimuth of the source with respect to azimuth of the wind:

$$\varkappa \equiv \varrho_{\text{source}} - \varrho_{\text{wind}}.$$

Let $\boldsymbol{u_i}$ be a unit vector (a_i, b_i, c_i) along the incident ray pointing from source to origin.

The Detector

The outgoing ray is also bent in the vertical direction due to the effects of refraction. Let θ be the zenith angle at the point of reflection of the outgoing ray, or, equivalently, the apparent zenith angle of the detector as observed from the origin. Let ϕ be the azimuth of the outgoing ray with respect to the azimuth of the wind at the point of reflection:

$$\phi \equiv \varrho_{\text{detector}} - \pi - \varrho_{\text{wind}}.$$

Let $\boldsymbol{u_r}$ be a unit vector (a_r, b_r, c_r) along the reflected ray pointing from origin to detector.

The Plane of Reflection

The plane of reflection will contain $\boldsymbol{u_i}$, $\boldsymbol{u_n}$, and $\boldsymbol{u_r}$. According to the law of reflection,

$$\boldsymbol{u_r} - \boldsymbol{u_i} = 2 \cos\Omega \, \boldsymbol{u_\varkappa} , \tag{1}$$

where Ω is the angle of incidence and the angle of reflection.

PROBLEM ONE

A major contribution to the signal reaching an infrared camera viewing the ocean is the radiance reflected into the camera from various portions of the sky. Each ocean facet will have its own tilt at any given moment and will be contributing a specular reflection from a unique part of the sky dome into the camera. In this situation, we want to know what part of the sky dome is coming into play for a given facet tilt and a given camera orientation. This leads us to our first problem: Assume that the detector orientation (θ, ϕ) is fixed with respect to the reflection point. Choose a facet slope (α, β). Demand a specular reflection by the facet from some portion of the sky (the source) into the camera (the detector). Problem one is to find equations for the angle of incidence (Ω) and the zenith angle of the source (μ) in terms of α, β, θ, and ϕ.

THE VECTOR COMPONENTS

We will follow the approach of Cox and Munk (1954) and first find the components of the three unit vectors that appear in the law of reflection.

The components for the unit normal to the facet are found by noting that for any vector $\boldsymbol{r} = (x, y, z)$ in the facet,

$$\boldsymbol{u_\varkappa} \cdot \boldsymbol{r} = a_n x + b_n y + c_n z = 0 \tag{2}$$

with

$$a_n^2 + b_n^2 + c_n^2 = 1 . \tag{3}$$

By evaluation of equation (2) in the x–z and y–z planes, the ratios a_n/c_n and b_n/c_n are determined, which sets the direction of the normal. Then c_n is found from equation (3), which sets the length of $\boldsymbol{u_n}$ to one.

The components of the incident unit vector and the reflected unit vector are found by resolving them first into components normal to the horizon (parallel to the z axis) and within the horizon, then resolving the horizontal component into its x and y values.

For the reflected ray,

$$\begin{aligned} a_r &= + \sin\theta \cos\phi \\ b_r &= - \sin\theta \sin\phi \\ c_r &= + \cos\theta \end{aligned} \tag{4}$$

For the incident ray,

$$
\begin{aligned}
a_i &= -\sin\mu\ \cos\varkappa \\
b_i &= +\sin\mu\ \sin\varkappa \\
c_i &= -\cos\mu
\end{aligned}
\tag{5}
$$

For the facet normal,

$$
\begin{aligned}
a_n &= -\tan\alpha\ \cos\gamma \\
b_n &= -\tan\beta\ \cos\gamma \\
c_n &= +\cos\gamma
\end{aligned}
\tag{6}
$$

where

$$\cos^2\gamma \equiv 1/(\tan^2\alpha + \tan^2\beta + 1)\,. \tag{7}$$

As shown in figure 1 in the main text, γ, the tilt, is the angle formed between the horizon and the direction of steepest ascent within the facet.

THE SOLUTION TO PROBLEM ONE

By rewriting the law of reflection as

$$-\boldsymbol{u}_i = 2\cos\Omega\ \boldsymbol{u}_n - \boldsymbol{u}_r \tag{8}$$

and squaring, we find that

$$\cos\Omega = \boldsymbol{u}_r\cdot\boldsymbol{u}_n = a_r a_n + b_r b_n + c_r c_n\,, \tag{9}$$

which gives an expression for cos Ω after substitution of the components from equations (4) and (6). The expression for cos μ is given by the z component of equation (8) after substitution of the components. The results are

$$
\begin{aligned}
\cos\Omega &= (-\sin\theta\ \cos\phi\ \tan\alpha + \sin\theta\ \sin\phi\ \tan\beta + \cos\theta)(\cos\gamma) \\
\cos\mu &= (-2\sin\theta\ \cos\phi\ \tan\alpha + 2\sin\theta\ \sin\phi\ \tan\beta - [\sec^2\gamma - 2]\cos\theta)(\cos^2\gamma) \\
\sec^2\gamma &\equiv \tan^2\alpha + \tan^2\beta + 1 = \tan^2\gamma + 1\,.
\end{aligned}
\tag{10}
$$

PROBLEM TWO

Another major contribution to the camera signal will be sun glint, wherein a solar ray is reflected into the camera by a wave facet. In this situation, we know the source and detector

positions but need to know the wave slope required for a specular reflection. This brings us to the next problem: Assume that the detector orientation (θ, ϕ) and the source orientation (μ, $\varkappa$) are both fixed with respect to the point of reflection. Demand a specular reflection by the facet from the source into the detector. Problem two is to find the angle of incidence (Ω) and the facet slopes ($\tan\alpha$, $\tan\beta$) in terms of θ, ϕ, μ, and $\varkappa$.

THE SOLUTION TO PROBLEM TWO

To find the angle of incidence, square equation (8) to obtain

$$2\cos^2\Omega = 1 - \boldsymbol{u}_r \cdot \boldsymbol{u}_i \tag{11}$$

and substitute component values for reflected and incident rays from equations (4) and (5), respectively. The facet slopes are found by evaluating the components of $\boldsymbol{u}_n$ in equation (1) by using equations (4) and (5) once again. The result is:

$$\begin{aligned}
\cos\Omega &= [(1 + \sin\theta\cos\phi\sin\mu\cos\varkappa + \sin\theta\sin\phi\sin\mu\sin\varkappa + \cos\theta\cos\mu)/2]^{1/2} \\
\tan\alpha &= (-\sin\theta\cos\phi - \sin\mu\cos\varkappa)/(\cos\theta + \cos\mu) \\
\tan\beta &= (+\sin\theta\sin\phi + \sin\mu\sin\varkappa)/(\cos\theta + \cos\mu) \\
\tan^2\gamma &\equiv \tan^2\alpha + \tan^2\beta\,.
\end{aligned} \tag{12}$$

For viewing toward the sun, $\phi = \varkappa - \pi$ and the above equations reduce to

$$\begin{aligned}
\Omega &= \frac{\mu + \theta}{2} \\
\tan\alpha &= +\cos\phi\tan\gamma \\
\tan\beta &= -\sin\phi\tan\gamma \\
\gamma &= \left|\frac{\mu - \theta}{2}\right|.
\end{aligned} \tag{13}$$

Some useful additional relationships are

$$\begin{aligned}
\cos\Omega &= [(1 + \sin\theta\sin\mu\cos(\phi - \varkappa) + \cos\theta\cos\mu)/2]^{1/2} \\
\cos(2\Omega) &= \sin\theta\sin\mu\cos(\phi - \varkappa) + \cos\theta\cos\mu \\
\cos\gamma &= (\cos\theta + \cos\mu)/2\cos\Omega\,.
\end{aligned} \tag{14}$$

SYMMETRIES

The signs of the components, hence the signs of the terms in equations (10) and (12), depend on what conventions are employed when the problem is setup. Two changes in the initial setup that might be considered are the following:

1. Change the sense of azimuth to one that is more natural for the *x–y–z* coordinate system; namely, measure azimuthal angles positive going *counterclockwise* looking

down on the horizon along the $-z$ direction. If this convention is adopted, all equations for the components remain the same except that the sign of the y–component is reversed for the incident and reflected rays:

$$b_r \rightarrow -b_r$$
$$b_i \rightarrow -b_i \tag{15}$$

2. Change the definition of ϕ to $\varrho_{detector} - \varrho_{wind}$ so that it gives the angle between the direction in which the camera is *pointed* and the direction of the wind. If this convention is adopted, then the equations for all components remain the same except that the signs for the x and y components of the reflected ray are reversed:

$$a_r \rightarrow -a_r$$
$$b_r \rightarrow -b_r \tag{16}$$

3. If both changes are adopted at the same time, then

$$a_r \rightarrow -a_r$$
$$b_i \rightarrow -b_i \tag{17}$$

and the solutions to problems one and two become respectively

$$\cos\Omega = (\sin\theta\cos\phi\tan\alpha + \sin\theta\sin\phi\tan\beta + \cos\theta)(\cos\gamma)$$
$$\cos\mu = (2\sin\theta\cos\phi\tan\alpha + 2\sin\theta\sin\phi\tan\beta[\sec^2\gamma - 2]\cos\theta)(\cos^2\gamma) \tag{18}$$
$$\sec^2\gamma = \tan^2\alpha + \tan^2\beta + 1$$

and

$$\cos\Omega = ([-\sin\theta\cos\phi\sin\mu\cos\varkappa - \sin\theta\sin\phi\sin\mu\sin\varkappa + \cos\theta\cos\mu]/2)^{1/2}$$
$$\tan\alpha = (+\sin\theta\sin\phi - \sin\mu\cos\varkappa)/(\sin\theta + \cos\mu) \tag{19}$$
$$\tan\beta = (+\sin\theta\sin\phi - \sin\mu\sin\varkappa)/(\cos\theta + \cos\mu)$$

COMPARISON WITH FORTRAN CODE

Problem one has previously been considered by Wollenweber (1988) and introduced into LOWTRAN 6 as a set of subroutines that account for the reflection of infrared sky radiance by ocean wave facets into an infrared camera. The equations for $\cos\Omega$ and $\cos\mu$ occur just after line 100 of the subroutine GEOPRO. The following table associates the terms in the FORTRAN code with the symbols used here:

FORTRAN[2]	ANEN	SX	SY	CAL	PSI	COW	OME	PHI
This work	$\sec^2\gamma$	$\tan\alpha$	$\tan\beta$	$\cos\Omega$	ϕ	$\cos\mu$	Ω	$\pi/2-\theta$

Furthermore, the code apparently adopts both of the changes mentioned in the previous section since CAL and COW both have positive first terms.

APPENDIX B

LIST OF SYMBOLS
Braces {} indicate subscripts

LATIN

a	x component of a unit vector **u**
{av}	Average
b	y component of a unit vector **u**
c	z component of a unit vector **u**
{c}	Camera; also Crosswind
C	Degree Centigrade
{e}	Extinction
H	Irradiance (W cm^{-2})
H_λ	Spectral irradiance (W cm^{-2} μm^{-1})
{i}	Incident
{n}	Normal
N	Radiance (W cm^{-2} str^{-1})
N_λ	Spectral radiance (W cm^{-2} str^{-1} μm^{-1})
p	Cox–Munk directional wave slope probability
q	Cox–Munk nondirectional wave slope probability
R	Reflectivity
{r}	Reflected
{s}	Sun
S	Saunders shadowing factor
u	Unit vector
{u}	Upwind
W	Wind speed (ms^{-1})

{w}	Wind
x	Upwind direction in the horizon at the point of reflection
y	Crosswind direction in the horizon at the point of reflection
z	Direction of the zenith at the point of reflection

GREEK

α	Angular slope of wave facet in x direction; also Real part of the optical index of refraction
β	Angular slope of wave facet in y direction; also imaginary part of the optical index of refraction
γ	Tilt, the angular slope in the direction of steepest facet ascent measured with respect to the horizon
θ	Zenith angle of reflected ray at the point of reflection
ν	Normalized elevation of reflected ray at point of reflection
$\varkappa$	Azimuth of sun with respect to azimuth of wind
λ	Wavelength (μm)
μ	Zenith angle of sun at point of reflection
ϱ	Azimuth, measured positive counterclockwise from true north looking down on the horizon
σ	Root mean square deviation
τ	Transmittance
Ω	Angle of incidence

REPORT DOCUMENTATION PAGE

Form Approved
OMB No. 0704-0188

Public reporting burden for this collection of information is estimated to average 1 hour per response, including the time for reviewing instructions, searching existing data sources, gathering and maintaining the data needed, and completing and reviewing the collection of information. Send comments regarding this burden estimate or any other aspect of this collection of information, including suggestions for reducing this burden, to Washington Headquarters Services, Directorate for Information Operations and Reports, 1215 Jefferson Davis Highway, Suite 1204, Arlington, VA 22202-4302, and to the Office of Management and Budget, Paperwork Reduction Project (0704-0188), Washington, DC 20503.

1. AGENCY USE ONLY *(Leave blank)*	2. REPORT DATE June 1993	3. REPORT TYPE AND DATES COVERED Final
4. TITLE AND SUBTITLE MARINE-MODIFIED LOWTRAN: THE CONTRIBUTION OF SUN GLINT		5. FUNDING NUMBERS PE: 062435N TA: RL3C–R035E82 WU: DN302215
6. AUTHOR(S) C. R. Zeisse		
7. PERFORMING ORGANIZATION NAME(S) AND ADDRESS(ES) Naval Command, Control and Ocean Surveillance Center (NCCOSC), RDT&E Division San Diego, CA 92152–5001		8. PERFORMING ORGANIZATION REPORT NUMBER TR 1611
9. SPONSORING/MONITORING AGENCY NAME(S) AND ADDRESS(ES) Naval Research Laboratory Detachment Stennis Space Center, Mississippi 39529–5000		10. SPONSORING/MONITORING AGENCY REPORT NUMBER
11. SUPPLEMENTARY NOTES		
12a. DISTRIBUTION/AVAILABILITY STATEMENT Authorized for public release; distribution is unlimited.		12b. DISTRIBUTION CODE

13. ABSTRACT *(Maximum 200 words)*

Personnel added sun glint to the Atmospheric Transmittance/Radiance Computer Code LOWTRAN 6 in order to provide a more realistic representation of the infrared marine environment. Personnel compared the modified model's results with infrared data that were taken at 3–5 microns over the open ocean during different solar elevations and wind speed conditions. A significant glint contribution was obtained at 1450 PDT on 10 October 1991. At this time, personnel noted a close match between the shape of the predicted and observed radiance values in the sky and sea. The absolute value of the predicted and observed radiances differed, however, by a large constant with an equivalent blackbody temperature of approximately 5°C. Personnel speculated that the origin of this additional radiance may be multiple scattering of solar radiation.

14. SUBJECT TERMS Sun glint spectral radiance LOWTRAN 6 infrared vision thermal imaging system			15. NUMBER OF PAGES 44 16. PRICE CODE
17. SECURITY CLASSIFICATION OF REPORT UNCLASSIFIED	18. SECURITY CLASSIFICATION OF THIS PAGE UNCLASSIFIED	19. SECURITY CLASSIFICATION OF ABSTRACT UNCLASSIFIED	20. LIMITATION OF ABSTRACT SAME AS REPORT